1    **Development of Narrow Spectrum ATP-competitive Kinase Inhibitors as Probes for**

2    **BIKE and AAK1**

3    Rafael M. Couñago[1], Alison D. Axtman[2,3], Stephen J. Capuzzi[3], Hátylas Azevedo[4], David H.

4    Drewry[2,3], Jonathan M. Elkins[1,5], Opher Gileadi[1,5], Cristiano R. W. Guimarães[4], Alessandra

5    Mascarello[4], Ricardo A. M. Serafim[1], Carrow I. Wells[2,3], Timothy M. Willson[2,3], William J.

6    Zuercher[2,3,*]

7    [1]Structural Genomics Consortium, Universidade Estadual de Campinas — UNICAMP,

8    Campinas, SP, Brazil.

9    [2]Structural Genomics Consortium, UNC Eshelman School of Pharmacy, University of

10   North Carolina at Chapel Hill, Chapel Hill, NC, USA.

11   [3]Division of Chemical Biology and Medicinal Chemistry, UNC Eshelman School of

12   Pharmacy, University of North Carolina at Chapel Hill, Chapel Hill, NC, USA.

13   [4]Aché Laboratórios Farmacêuticos SA, Guarulhos, SP, Brazil.

14   [5]Structural Genomics Consortium and Target Discovery Institute, Nuffield Department of

15   Clinical Medicine, University of Oxford, Old Road Campus Research Building, Oxford,

16   OX3 7DQ, UK.

17   *Correspondence to W. Zuercher, email: william.zuercher@unc.edu

18    **ABSTRACT**: Understanding the structural determinants of inhibitor selectivity would

19    facilitate the design and preparation of kinase probes. We describe a pair of matched

20    compounds differing only by one degree of saturation but showing dramatic differential

21    activities at select kinases. We utilized x-ray crystallography and computational analysis

22    to rationalize the basis of the differential activity.


23    **INTRODUCTION**


24    The human protein kinases are a family of over 500 enzymes that are involved in critical

25    aspects of cell signaling but are often dysregulated in disease, especially cancer [1].

26    Protein kinases catalyze the transfer of phosphate from the cofactor ATP to their

27    substrate proteins. Although ATP-competitive protein kinase inhibitors have been

28    successfully developed to treat a range of cancers, inflammatory and fibrotic diseases,

29    the function of a large number of the enzymes remains unknown [2]. Potent and

30    selective small molecule inhibitors are powerful tools to probe the biology of these

31    understudied kinases [3].


32    Because ATP-competitive inhibitors bind to a common active site, they often show

33    activity across multiple kinases. For example, staurosporine inhibits more than 200

34    protein kinases. These broad spectrum inhibitors are useful for initial biochemical

35    characterization but have little utility as probes of kinase biology [4]. By contrast, other

36    ATP-competitive inhibitors possess activity on only a handful of kinases. These narrow

37    spectrum inhibitors have found utility in exploring the function of several historically

38    understudied kinases [5].


2

39  To strengthen the conclusions drawn from use of narrow spectrum kinase inhibitors, a

40  recently established best practice is to use the probe molecule in parallel with a

41  negative control, a closely-related analogue that is inactive for the target kinase [6].

42  Demonstration of divergent results between the probe inhibitor and its negative control

43  increases confidence that the engagement of the target kinase was responsible for the
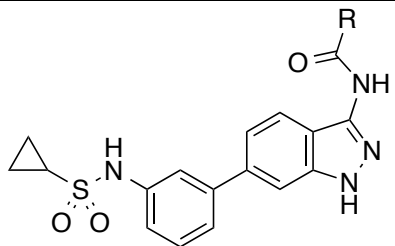
44  observed biology.

45  For ATP-competitive kinase inhibitors, a systematic approach to develop negative

46  control analogs is to synthesize a molecule that lacks the ability to form the critical hinge

47  binding interaction, typically composed of one or more hydrogen bonds with the highly

48  conserved hinge region in the enzyme [7]. These modifications result in "kinase dead"

49  analogues. Unfortunately, kinase dead analogues often lose affinity not only for the

50  primary target kinase but also for all other off-target kinases. New strategies to create

51  kinase probe negative controls that lose affinity selectively for their target kinase are

52  needed.

53  Here we describe a pair of compounds in which a minor structural change—namely, the

54  inclusion of a cyclopropyl versus an isopropyl substituent proximal to the hinge-binding

55  moiety—leads to unexpectedly large changes in activity within a small subset of protein

56  kinases but no change against many others. We used X-ray crystallography and

57  computational models to study the molecular basis for these differential effects on

58  affinity within the target and off-target kinases in an attempt to define general

59  approaches to design selective negative control analogs.

60  **RESULTS**

61  As part of a large-scale selectivity screen of ATP-mimetic kinase inhibitors, we identified

62  a pair of very closely related 3-acylaminoindazoles (**1** and **2**) that displayed a narrow

63  binding spectrum in the KINOMEscan panel of over 400 human protein kinase assays at

64  an inhibitor concentration of 1 μM (**S1 Table**). Structurally, **1** and **2** differed only by the

65  addition of two hydrogen atoms in the change from a cyclopropyl to isopropyl

66  carboxamide. **1** and **2** had several common kinase targets but also showed some degree

67  of divergence in kinase affinity profiles. A more detailed analysis of their binding

68  characteristics revealed that **1** had submicromolar affinity for 11 kinases and weaker

69  affinity for 2 additional kinases (**Table 1**), while **2** showed submicromolar affinity for

70  7/11 of the primary kinase targets and 1/2 of the minor targets. For most of these

71  kinases, only marginal differences in potency were observed between the analogs (<3-

72  fold). However, four kinases (AAK1, BIKE, RIOK1, and RIOK3) displayed remarkable

73  differential affinity between the cyclopropyl analog **1** and isopropyl analog **2** with a

74  preference for the former (27–150-fold).

75  **Table 1**. $K_d$ values for selected kinases. $K_d$ values were determined for kinases observed

76  to have >70% displacement of immobilized ligand with either **1** or **2** in a KINOMEscan

77  screen at 1 μM compound.

| Kinase | | $K_d$ Ratio 2:1 |
|---|---|---|
| |  | |

|  | 1 (R = cyclopropyl) $K_d$ (nM) | 2 (R = i-Pr) $K_d$ (nM) |  |
|---|---|---|---|
| AAK1 | 71 | 8800 | 124 |
| BIKE | 68 | >10000 | >150 |
| BRAF | 100 | 52 | 0.52 |
| RIOK1 | 170 | 9600 | 56 |
| PDGFRB | 250 | 61 | 0.24 |
| KIT | 290 | 77 | 0.27 |
| RIOK3 | 300 | 8200 | 27 |
| DDR1 | 400 | 150 | 0.38 |
| ABL1 | 540 | 190 | 0.35 |
| RAF1 | 580 | 350 | 0.60 |
| PDGFRA | 590 | 240 | 0.41 |
| CSF1R | 2000 | 1600 | 0.80 |
| p38a | 6900 | 550 | 0.08 |

78

79    AAK1 and BIKE, along with the related GAK and STK16, comprise the Numb-associated

80    kinase (NAK) subfamily of protein kinases [8]. NAK family members have been proposed

81    as potential drug targets for a wide range of therapeutic areas, including virology,

82    oncology, neurology, and ophthalmology [9-12]. In contrast, relatively little is known

83    about the relevance to cellular processes of the atypical kinases RIOK1 and RIOK3.

84    Accordingly, to explore the molecular basis of the remarkable differential activities of **1**

85    and **2**, we decided to study their interaction with the NAK family kinases. **1** and **2** were

86    evaluated in FRET-based ligand binding displacement assays for all four NAK family

87    members [13]. The cyclopropyl analog **1** showed >300-fold higher affinity for AAK1 and

88    BIKE relative to the isopropyl analog **2** (**Table 2**). Both compounds demonstrated weaker

89    affinity for GAK and STK16, although a >50-fold preference for **1** relative to **2** was

90    observed with the latter kinase.

91    **Table 2**. NAK family FRET-based binding displacement assay results.

| Kinase | $K_i$ (nM) | | Ratio |
|---|---|---|---|
| | 1 | 2 | |
| AAK1 | 8.3 | 2700 | 320 |
| BIKE | 13 | 3100 | 240 |
| GAK | 1600 | 4900 | 3 |
| STK16 | 330 | 19000 | 58 |

92

93    *Structural analysis of compound 1 binding*. BIKE and AAK1 are the closest members

94    within the NAK family and share a high sequence identity—74% over their kinase

95    domains and 81% within their ATP-binding sites. In order to obtain insights into the

96    molecular details of ligand interactions with these kinases, we determined the cocrystal

97    structure of BIKE kinase domain bound to compound **1** (**Table 3**), reasoning that both

98    kinases are likely to interact with **1** and **2** in similar manners.

99    **Table 3**. Crystal structure data collection and refinement statistics.

| Protein | BIKE |
|---|---|
| Ligand | **1** |
| X-ray source | DLS I02 |
| a (Å) | 41.96 |
| b (Å) | 111.15 |
| c (Å) | 164.05 |
| α, β, γ (°) | 90, 90, 90 |
| Space group | I 2 2 2 |
| Wavelength (Å) | 0.97949 |
| Resolution limit (Å)* | 28.6-2.41 (2.50-2.41) |
| Number of observations* | 81.078 (7.855) |
| Completeness (%)* | 99.1 (95.2) |
| Multiplicity* | 5.3 (5.2) |
| Rmerge (%)* | 0.074 (0.49) |
| Mean I/σI * | 13.2 (3.1) |
| Refinement | |
| Resolution Range (Å) | 21.75-2.41 |

6

| | |
|---|---|
| Rcryst | 0.176 |
| Rfree | 0.216 |
| No. protein atoms | 2,317 |
| No. ligand atoms | 28 |
| No. solvent atoms | 89 |
| Mean B-factor ($\text{Å}$) | 53.1 |
| Rmsd bond lengths ($\text{Å}$) | 0.010 |
| Rmsd bond angles (°) | 1.04 |
| Ramachandran statistics (%) | |
| Favored | 98.3 |
| Allowed | 1.7 |
| Outlier | 0 |
| PDB ID | 5IKW |
| Crystallization conditions | 10% (v/v) Broad MW PEG smear, 3.2 M $MgCl_2$, 100 mM Hepes pH 7.0 |

100    * Highest resolution shell shown in parentheses.

101    BIKE-**1** crystals diffracted to 2.4 $\text{Å}$ and contained a single protein chain per asymmetric

102    unit (chain A). Sorrell and colleagues have recently reported the structural

103    characterization of all four NAK family member kinase domains, including BIKE and AAK1

104    [8]. As previously observed, our structure of BIKE displayed a catalytically-competent

105    conformation in which residues in the protein regulatory spine ("R spine"; residues M99,

106    Y111, H178 and F199) are aligned and side-chain atoms from conserved residues in β3

107    and α-C (K79 and E95, respectively) form an ion pair [14, 15]. Moreover, the NAK family-

108    exclusive helical domain (P209 to Y224) found C-terminal of the activation segment

109    (from [198]DFG to APE[233] domains), dubbed ASCH (activation segment C-terminal helix) [8,

110    16, 17], also displayed an identical conformation in the BIKE structure described here

111    (**Figure 1a**).

7

112    **Figure 1.** Crystallographic characterization of BIKE bound to 3-acylaminoindazole **1**. (**a**)

113    BIKE-**1** adopts an active conformation. Protein (cartoon) regions important for activity

114    and ligand interaction are indicated and highlighted in different colors. As for other

115    NAK-family members, the activation segment of BIKE (orange) contains a C-terminal

116    helical segment (ASCH; in red). Inhibitor **1** (carbon atoms in pink) and BIKE residues

117    (carbon atoms in yellow) taking part in the regulatory hydrophobic spine and the critical

118    ion pair leading to an active conformation are shown as sticks. (**b**) Details of the BIKE-**1**

119    interactions. Inhibitor **1** is anchored to the hinge (green ribbon) via hydrogen bonds

120    (dashed lines) and complements the hydrophobic cavity formed by aliphatic side chains

121    from p-loop (purple ribbon) and β-6 residues. Potential interactions between main chain

122    carbonyl and the cyclopropane group are indicated by dashed lines. Hydrogen bonds

123    between Asn185, Gln137 and the sulfonamide group are also shown (dashed lines). (**c**)

124    Superposition of NAK family proteins AAK1 (blue; PDB ID 4WSQ), BIKE (grey, PDB IDs

125    5IKW, this work), GAK (PDB ID 4Y8D) and MPSK1 (PDB ID 2BUJ) shows variation in the p-

126    loop region despite good alignment in the hinge region. Compound anchoring hydrogen

127    bonds are shown for BIKE and **1** (sticks). (**d**) Electron density (2Fo-Fc) maps (grey mash;

128    1.0 σ contour) for **1**. (**e**) Primary sequence comparison of NAK family hinge and P-loop

129    regions.

130    The cocrystal structure of **1** and BIKE reveals that 3-acylaminoindazole **1** is anchored to

131    the protein hinge region (BIKE residues 131-137) *via* hydrogen bonds between the N

132    atoms of the indazole group and main chain carbonyl and NH groups of residues G131

133    and C133, respectively. An additional hydrogen bond is made between the amino group

134   of **1** and the carbonyl group of C133. At the other end of the inhibitor, the sulfonamide

135   group engages residues Q137 and N185 via hydrogen bonds. These interactions position

136   the pendant aliphatic group into a hydrophobic cavity within the P-loop formed by

137   residues V65 and S65. The indazole and the aniline rings are not coplanar to each other.

138   This flexibility provides excellent shape-complementarity between the inhibitor and the

139   ATP-binding pocket; especially with the aliphatic side chains from L187 and from p-loop

140   residues L57, A58 and V65. There is also a sulfur-$\pi$ interaction between the aniline ring

141   and the sulfur atom of C197 (**Figure 1b**). Residue C197 is adjacent to the protein DFG

142   motif and has been proposed as a site of covalent modification by the inhibitor (5*Z*)-7-

143   oxozeaenol [8]. The cyclopropane group adjacent to the carboxyl group in **1** is

144   accommodated within a sharp turn of the peptide backbone involving residues

145   occupying positions +3, +4 and +5 from the so-called gatekeeper, or GK, residue (M130

146   in BIKE). This kink in the peptide backbone allows the carbonyl groups of residues GK+3

147   (C133) and GK+4 (R134) to point towards the cyclopropyl C-H group, approaching at a

148   distance of 3.6 and 3.3 Å, respectively (**Figure 1b**).

149   We compared our BIKE-**1** structure with published structures of DDR1 (PDB: 5FDP),

150   BRAF (PDB: 4XV9), AAK1 (PDB: 4WSQ), and RIOK1 (PDB: 4OTP) to attempt to rationalize

151   the structural basis differential activity of **1** and **2** on some but not all kinases. Surface

152   electrostatic potential is quite different for kinases that show differential activity

153   compared with those that do not. AAK1, BIKE, and RIOK1 have bland surface charge

154   where the critical cyclopropyl moiety of **1** is accommodated within the binding pocket.

9

155 In contrast, BRAF and DDR1 have highly charged surfaces around their

156 corresponding hinge binding regions.

157 Superimposing our BIKE-**1** structure with the previously published structures from the

158 NAK family [8] by aligning the hinge residues (rmsd < 0.3 Å for 7 equivalent Cα) revealed

159 that the P-loop of STK16 and GAK are substantially displaced compared to the position

160 occupied by this region in BIKE and AAK1 structures (**Figure 1d**). The extensive contacts

161 **1** makes with the P-loop may explain its selectivity for BIKE and AAK1 over the other two

162 members of the NAK family. Interestingly, the primary sequence alignment of NAK

163 family members reveals that sequence conservation is high for the P-loop region and

164 low for the hinge moiety (**Figure 1e**).

165 *Computational studies*. A range of computational methodologies was applied to shed

166 light on the differential affinities of **1** and **2**. Energy minimization calculations in the

167 unbound state using the OPLS3 force field [18] and the GB/SA [19] solvation model

168 suggest that dehydration penalty upon binding is not a dominant factor, as similar

169 hydration values were obtained for **1** (-29.8 kcal/mol) versus **2** (-29.2 kcal/mol); the

170 cyclopropyl analog was actually slightly more penalized. To investigate the electronic

171 properties, electrostatic potential derived atomic charges using the B3LYP exchange-

172 correlation energy functional [20] and the 6-31G** basis set [21] were obtained in the

173 gas phase. In this case, striking differences were observed for the C-H bond adjacent to

174 the carbonyl group; it was much more polarized for cyclopropyl than isopropyl (**Figure**

175 **2**), with no major differences for the adjacent amide.

176   **Figure 2.** Computationally generated electrostatic potential (ESP) derived atomic

177   charges for (A) **2** and (B) **1**.

178   Beyond defining potential enthalpic differences between cyclopropyl and isopropyl

179   substituents, we also investigated possible entropic differences between **1** and **2** for

180   selected kinases. The Glide docking application was used to predict binding poses in

181   each investigated kinase, and the components of entropy change (translational,

182   rotational, and vibrational) upon binding of **1** and **2** to the kinases were calculated using

183   the RRHO approximation (**Table 4**). Translational and rotational entropic losses were

184   essentially equivalent for **1** and **2** at any given kinase. However, the vibrational entropic

185   gain was higher for **1** with all kinases except p38α. Interestingly, upon binding, the

186   largest overall changes in entropy, or $\Delta(T\Delta S_{bind})$, between **1** and **2** were observed for

187   AAK**1** and BIKE. These two kinases displayed the two largest $K_d$ ratios. $\Delta(T\Delta S_{bind})$

188   between **1** and **2** was markedly lower for those kinases not displaying significant activity

189   cliffs. However, there are two exceptions to this observation, namely KIT and RIOK1. The

190   former displayed a significant $\Delta(T\Delta S_{bind})$ between **1** and **2**, although there is not a

191   significant difference in affinity. With RIOK**1**, the entropic difference between **1** and **2**

192   was modest, despite a $K_d$ ratio **2:1** of 56 (**Table 1**).

193   **Table 4.** Thermodynamic parameters of binding **1** and **2** with kinases.

| Kinase | PDB | Cmpd | $T\Delta S_{bind}$ | | | | $\Delta(T\Delta S_{bind})$ |
|--------|-----|------|-------|-----|-----|-------|--------------------------|
|        |     |      | Trans | Rot | Vib | Total |                          |
| AAK1   | 5L4Q | 1   | -11.30 | -11.14 | 4.70 | -17.75 | 3.54 |
|        |     | 2    | -11.31 | -11.07 | 1.09 | -21.29 |       |
| BIKE   | 5IKW | 1   | -11.30 | -11.07 | 4.64 | -17.73 | 2.51 |
|        |     | 2    | -11.31 | -11.10 | 2.17 | -20.24 |       |

11

| | | | | | | | |
|---|---|---|---|---|---|---|---|
| p38a | 5LAR | 1 | -11.30 | -11.13 | 3.35 | -19.09 | -0.10 |
| | | 2 | -11.31 | -11.17 | 3.49 | -18.98 | |
| ABL | 4ZOG | 1 | -11.30 | -11.05 | 3.15 | -19.20 | 1.64 |
| | | 2 | -11.31 | -11.04 | 1.51 | -20.84 | |
| KIT | 4U0I | 1 | -11.30 | -11.13 | 3.09 | -19.34 | 3.23 |
| | | 2 | -11.31 | -11.18 | -0.08 | -22.57 | |
| DDR1 | 5FDP | 1 | -11.30 | -11.06 | 3.84 | -18.52 | 1.45 |
| | | 2 | -11.31 | -11.08 | 2.41 | -19.97 | |
| CSF1R | 4R7H | 1 | -11.30 | -11.10 | 2.21 | -20.19 | 1.07 |
| | | 2 | -11.31 | -11.10 | 1.14 | -21.27 | |
| RIOK1 | 4OTP | 1 | -11.30 | -11.03 | 6.66 | -15.68 | 0.64 |
| | | 2 | -11.31 | -11.10 | 6.09 | -16.32 | |
| RAF1 | 3OMV | 1 | -11.30 | -11.06 | 2.82 | -19.54 | 1.52 |
| | | 2 | -11.31 | -11.09 | 1.34 | -21.06 | |

194
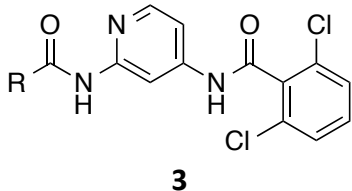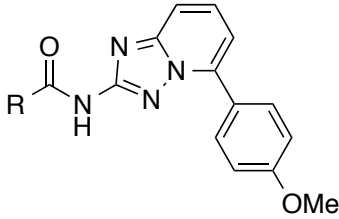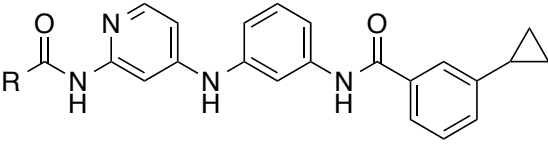
## DISCUSSION

196    The term "activity cliff" has been proposed to describe pairs of structurally similar

197    compounds, like **1** and **2**, with a large difference in potency relative to a common target

198    [22]. There have been other reports of kinase inhibitor activity cliffs involving

199    cyclopropyl and isopropyl carboxamides proximal to their hinge binding moiety (**Table**

200    **5**). The 2-cyclopropylcarboxamidopyridine **3a** showed >100x higher affinity for TYK2

201    than the isopropyl analog **3b** [23]. This effect is not limited to binding assays as

202    triazolopyrimidines **4** show >100x difference $IC_{50}$ value in a JAK1 biochemical activity

203    assay [24]. Similarly, **5a** displayed a much higher inhibition potency than **5b** in an

204    enzymatic activity assay of mutant B-Raf$^{V600E}$ activity [25]. These examples substantiate

205    our observations that subtle changes in structure can lead to selective inhibition of

206    specific protein kinases. To the best of our knowledge, **3**-**5** were not subjected to broad

12

207    kinome activity characterization, and the breadth of the associated activity cliffs has not

208    been evaluated.

209    **Table 5.** Previously reported matched pairs of kinase inhibitors demonstrating an affinity

210    or activity cliff between cyclopropyl and isopropyl compounds.

211

| Structure | Activity |
|---|---|
|   **3** | TYK2 $K_i$  **3a** R = Cyclopropyl: 4.8 nM  **3b** = Isopropyl: 840 nM  Ref: [23] |
|   **4** | JAK1 $IC_{50}$  **4a**: R = Cyclopropyl: 60 nM  **4b**: R = Isopropyl: >10000 nM  Ref: [24] |
|   **5** | B-Raf$^{V600E}$ $IC_{50}$  **5a**: R = Cyclopropyl: 35 nM  **5b**: R = Isopropyl: 420 nM  Ref: [25] |

212

213    The cyclopropyl ring is a versatile lipophilic group that frequently appears in preclinical

214    and clinical candidate molecules. It has been described to have "magical" properties

215    that can enhance potency, reduce off-target effects, increase metabolic stability and

216    brain permeability, yet the precise molecular basis for these effects remains poorly

217    understood [26]. Theoretical studies on cyclopropane and its derivatives suggest that

218    atomic bonding results mainly from the overlap of three $sp^2$ hybrids (one on each

219    carbon) pointing towards the center of the ring. Thus, the electron distribution in the C-

13

220 C internuclear region is not concentrated along the line between the nuclei, but rather

221 slightly outside this line. As a consequence, the C-C bonds have enhanced $\pi$ character,

222 and the C-H bonds have more *s* character. In other words, the cyclopropyl ring behaves

223 much like an alkene, interacts with neighboring $\pi$-electron systems, and has CH bonds

224 with increased acidity relative to standard alkanes [27]. These effects are apparent

225 when the emerging negative charge on the C-H carbon is stabilized by conjugation, such

226 as the one between the $\pi$-like cyclopropyl and an amide carbonyl group in **1**. Calculated

227 electrostatic potential charges, as demonstrated above, may contribute to the activity

228 difference between **1** and **2**.

229 3-Acylaminoindazoles are a known class of ATP-competitive protein kinase inhibitors

230 [28]. The heterocyclic core mimics the adenosine base of ATP and forms hydrogen

231 bonds with the hinge motif of the enzyme. **1** and **2**, differing by only two hydrogen

232 atoms were screened across 400 human protein kinases to define both compounds as

233 narrow spectrum inhibitors, with high affinity binding to <3% of the kinases surveyed.

234 Both **1** and **2** bound to seven kinases (ABL1, BRAF, DDR1, KIT, PDGFRA, PDGFRB, and

235 RAF1) with submicromolar affinity. Surprisingly, cyclopropyl amide **1** bound to an

236 additional four kinases (AAK1, BIKE, RIOK1, and RIOK3) where isopropyl amide **2** was not

237 effective. Thus, this pair of ATP-competitive kinase inhibitors have the potential to be

238 used to probe selectively the biology of just 4 protein kinases while controlling for over

239 400 others in the human genome.

240   BIKE and AAK1 are both members of the NAK (Numb-associated kinase) family of

241   protein kinases and share close sequence identity within their catalytic sites. Both

242   kinases are potently inhibited by the 3-acylaminoindazole **1** and are likely to interact

243   with the inhibitor through conserved interactions. The BIKE-**1** cocrystal structure

244   provides a clear view into the molecular details of the enzyme-ligand interaction. The

245   critical cyclopropyl carboxamide sits in a pocket adjacent to the hinge-binding residues

246   and is orientated toward the protein surface. The amide NH of **1** and the cyclopropyl

247   ring C-H sit in close proximity (2.70 and 3.29 Å, respectively) to the Cys133 carbonyl

248   oxygen (**Figure 3**). Our quantum mechanical calculations showed that the cyclopropyl

249   group has an increased polarization across the ring C-H compared the corresponding

250   isopropyl analogue. The complex between the cyclopropyl derivative **1** and BIKE is

251   indicative of a CH-O nonconventional hydrogen bond. Electrostatic interactions

252   dominate hydrogen bonds and the increased polarization of the cyclopropyl C-H bond,

253   as evidenced by the electrostatic potential charges, may explain why **1** shows

254   significantly higher affinity for AAK1 and BIKE than the isopropyl analog **2** but leaves

255   unanswered the question about why **1** and **2** are equipotent at other kinases.

256   **Figure 3.** (A) **1** bound in BIKE active site. (B) Two dimensional compound interaction

257   diagram of **1** and BIKE depicting adjacent residues and key interactions.

258   Modulating entropy contributions has previously been proposed as a means to increase

259   binding affinity between small molecules and proteins [29]. Upon binding, ligands lose

260   degrees of freedom with respect to translational, rotational, and vibrational motion.

15

261   This loss of freedom constitutes a loss of entropy, which disfavors binding. Given its

262   triangular nature and smaller size, the cyclopropyl group may vibrate more freely within

263   the protein, which favor binding when compared to the isopropyl group. Importantly,

264   depending on the protein environment and architecture, this effect can be more

265   pronounced. In our cocrystal structure of BIKE and **1**, the cyclopropyl group of interest is

266   more solvent exposed. As such, this group is not as restricted by the binding site and

267   does not experience a significant loss in vibrational entropy, which may be driving the

268   activity cliff observed between **1** and **2**. Kinases for which an activity cliff between **1** and

269   **2** is not observed may have the cyclopropyl group less solvent exposed, leading to a

270   larger vibrational entropy loss.

271   We have suggested that differences in electrostatic potential or in vibrational entropy

272   changes may help to rationalize the activity cliffs between **1** and **2** in some kinases but

273   not in others. We recognize that there are myriad other subtle changes in the binding

274   pockets that must also be explored to enable prediction of which kinases can be

275   differentially inhibited by matched ligand pairs like **1** and **2**. Our enhanced

276   understanding of the differential interactions of **1** and **2** within the binding pockets of

277   AAK1, BIKE, and other kinases will improve our ability to produce narrow spectrum

278   probes with optimal negative control analogs for use in biological studies.

279   **Supporting Information**

280   **S1 Table. Results of KINOMEscan and select $K_d$ determinations for 1 and 2.**

281   KINOMEscan assay panel and associated $K_d$ determinations were conducted at

282    DiscoverX Corporation. Compounds were evaluated as single measurements at 1 μM.

283    Displacement percentage ("Disp %") reflects the extent to which the compound

284    displaced the kinase construct from an immobilized ligand. $K_d$ values were determined

285    for all kinases with ≥70% displacement with **1** in the KINOMEscan screen at 1 μM

286    compound and selected other kinases.

287    **MATERIALS AND METHODS**

288    *N*-(6-(3-(cyclopropanesulfonamido)phenyl)-1*H*-indazol-3-yl)cyclopropanecarboxamide

289    (**1**). $^1$H NMR (400 MHz, Methanol-$d_4$) δ 7.83 − 7.78 (d, *J* = 8.6 Hz, 1H), 7.61 − 7.54 (m,

290    2H), 7.46 − 7.30 (m, 3H), 7.29 − 7.23 (ddd, *J* = 7.7, 2.2, 1.3 Hz, 1H), 2.62 − 2.49 (tt, *J* = 8.0,

291    4.8 Hz, 1H), 1.95 − 1.84 (ddd, *J* = 12.5, 7.9, 4.2 Hz, 1H), 1.07 − 0.77 (m, 8H). MS+ (− ES

292    API) - 397.1

293    *N*-(6-(3-(cyclopropanesulfonamido)phenyl)-1*H*-indazol-3-yl)isobutyramide (**2**). $^1$H NMR

294    (400 MHz, Methanol-$d_4$) δ 7.82 − 7.75 (d, *J* = 8.6 Hz, 1H), 7.62 − 7.54 (dt, *J* = 10.9, 1.5 Hz,

295    2H), 7.47 − 7.31 (m, 3H), 7.31 − 7.22 (ddd, *J* = 7.8, 2.2, 1.3 Hz, 1H), 2.84 − 2.69 (hept, *J* =

296    6.8 Hz, 1H), 2.61 − 2.50 (tt, *J* = 8.0, 4.8 Hz, 1H), 1.29 − 1.15 (d, *J* = 6.8 Hz, 6H), 1.14 − 0.82

297    (m, 4H).  MS+ (− ES API) - 399.1

298    **DiscoverX kinase affinity measurements.** KINOMEscan assay panel profiling and

299    associated $K_d$ determinations were obtained at DiscoverX Corporation using their

300    previously described methodology [30, 31].

301 **Binding displacement assays.** Inhibitor binding was determined using a binding-

302 displacement assay, which tests the ability of the inhibitors to displace a fluorescent

303 tracer compound from the ATP binding site of the kinase domain. Inhibitors were

304 dissolved in DMSO and dispensed as 16-point, 2x serial dilutions in duplicate into black

305 multiwell plates (Greiner). Each well contained either 0.5 nM or 1 nM biotinylated

306 kinase domain protein ligated to streptavidin-Tb-cryptate (Cisbio), 12.5 nM or 25 nM

307 Kinase Tracer 236 (ThermoFisher Scientific), 10 mM Hepes pH 7.5, 150 mM NaCl, 2 mM

308 DTT, 0.01% BSA, 0.01% Tween-20. Final assay volume for each data point was 5 µL, and

309 final DMSO concentration was 1%. The plate was incubated at room temperature for 1.5

310 hours and then read using a TR-FRET protocol on a PheraStarFS plate reader (BMG

311 Labtech). The data was normalized to 0% and 100% inhibition control values and fitted

312 to a four parameter dose-response binding curve in GraphPad Software. The

313 determined $IC_{50}$ values were converted to $K_i$ values using the Cheng-Prusoff equation

314 and the concentration and $K_d$ values for the tracer (previously determined).

315 **Cloning, Expression, Purification and crystallization**. BIKE$_{38\text{-}345}$ $_{(K320A, K321A)}$ with a tobacco

316 etch virus (TEV) protease cleavable, N-terminal 6xHis tag was expressed from vector

317 pNIC-ZB. To improve BIKE crystallization, a cluster of surface entropy reduction

318 mutations [32] was engineered into the expression construct, K320A/K321A [8]. For

319 protein production, the host *E. coli* strain, BL21(DE3)-R3 expressing lambda

320 phosphatase, was cultivated in TB medium (+ 50 µg/ml kanamycin, 35 µg/ml

321 chloramphenicol) at 37$^o$C until OD$_{600}$ reached ~3 and then cooled to 18$^o$C for 1 hour.

322 Isopropyl 1-thio-D-galactopyranoside was added to 0.1 mM, and growth continued at

323     18$^o$C overnight. The cells were collected by centrifugation then resuspended in 2x lysis

324     buffer (100 mM HEPES buffer, pH 7.5, 1.0 M NaCl, 20 mM imidazole, 1.0 mM tris(2-

325     carboxyethyl)phosphine, 2x Protease Inhibitors Cocktail Set VII (Calbiochem, 1/1000

326     dilution) and flash-frozen in liquid nitrogen. Cells were lysed by sonication on ice. The

327     resulting proteins were purified using Ni-Sepharose resin (GE Healthcare) and eluted

328     stepwise in binding buffer with 300 mM imidazole. Removal of the hexahistidine tag was

329     performed at 4$^o$C overnight using recombinant TEV protease. Proteins were further

330     purified using reverse affinity chromatography on Ni-Sepharose followed by gel

331     filtration (Superdex 200 16/60, GE Healthcare). Protein in gel filtration buffer (25 mM

332     HEPES, 500 mM NaCl, 0.5 mM TCEP, 5% [v/v] glycerol) was concentrated to 12 mg/ml

333     using 30 kDa MWCO centrifugal concentrators (Millipore) at 4$^o$C. 3-acylaminoindazole **1**

334     in 100% DMSO was added to the protein in a 3-fold molar excess and incubated on ice

335     for approximately 30 minutes. The mixture was centrifuged at 14,000 rpm for 10

336     minutes at 4$^o$C prior to setting up 150 nL volume sitting drops at three ratios (2:1, 1:1, or

337     1:2 protein-inhibitor complex to reservoir solution). Crystallization experiments were

338     performed at 20°C. Crystals were cryoprotected in mother liquor supplemented with 20-

339     25% glycerol before flash-freezing in liquid nitrogen for data collection. Diffraction data

340     were collected at the Diamond Light Source. The best diffracting crystals grew under the

341     conditions described in **Table 1**. When noted, crystal optimization used Newman's

342     buffer system [33] and defined PEG smears [34].

343     **Structure Solution and Refinement.** Diffraction data were integrated using XDS [35] and

344     scaled using AIMLESS from the CCP4 software suite [36]. Molecular replacement for was

345   performed with Phaser [37] using BIKE/AZD7762 (PDB ID: 4W9W) [8] as a search model.

346   Automated model building was performed with Buccanner [38]. Automated refinement

347   was performed in PHENIX [39]. Coot [40] was used for manual model building and

348   refinement. Structure validation was performed using MolProbity [41]. Structure factors

349   and coordinates have been deposited in the PDB (see Table 1).

350   **Computation**. Solvation free energies and quantum mechanical calculations were run

351   using Macromodel ([42]) and Jaguar ([43]) from Schrodinger Inc. Further computational

352   studies were performed using Maestro 11 from Schrodinger (Schrödinger Release 2016-

353   4: Maestro, Schrödinger, LLC, New York, NY, 2016). The lowest energy configurations for

354   compounds **1** and **2** at pH 7 were generated with the Ligand Preparation application

355   (Schrödinger Release 2016-4: LigPrep, Schrödinger, LLC, New York, NY, 2016). Next, PDB

356   crystal structures for AAK1, BIKE and the other kinases in Table 4 were downloaded and

357   prepared for docking. Briefly, bond orders were assigned, hydrogen atoms were added,

358   selenomethionine residues were converted to methionines, and missing side chains

359   were filled with the Prime application. The protein grid for docking was set by selecting

360   the center of the cocrystal ligand in the PDB structure.  The Glide application was used

361   for docking of 1 and 2 to all kinases (Schrödinger Release 2016-4: Glide, Schrödinger,

362   LLC, New York, NY, 2016.). Flexible ligand sampling was allowed with the XP (extra

363   precision) scoring function (http://pubs.acs.org/doi/abs/10.1021/jm051256o). Once the

364   ligands were docked and the lowest energy poses were retrieved, a Rigid Rotor

365   Harmonic Oscillation (RRHO) approximation was performed on the theoretical protein-
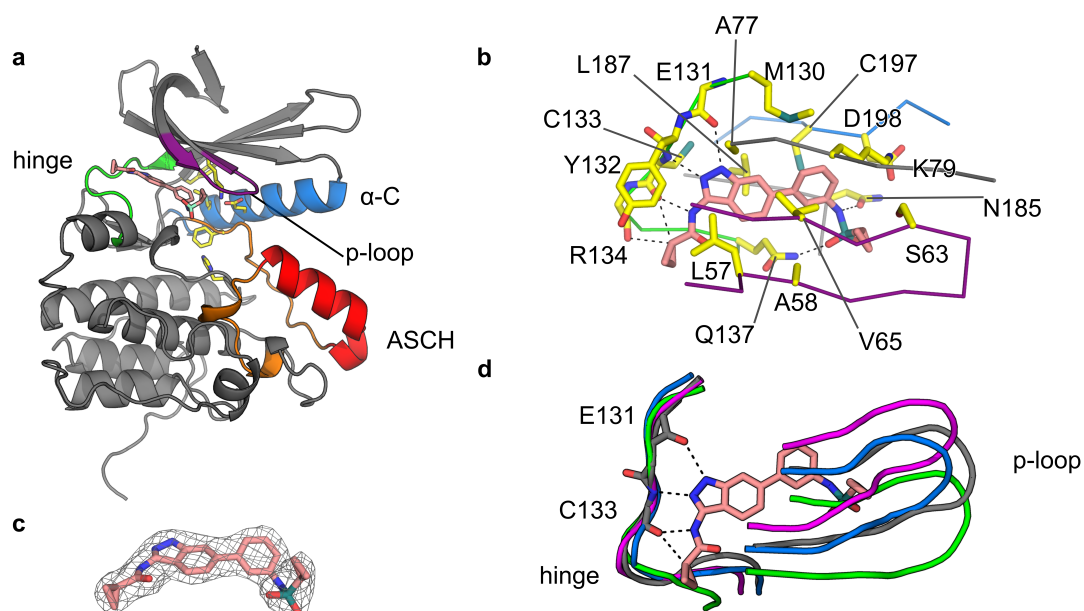
366   ligand  complex  (https://www.ncbi.nlm.nih.gov/pmc/articles/PMC3329805/).  For  the

367   RRHO   approximation,   an   OPLS_2005   force   field   was   applied

368   (http://pubs.acs.org/doi/abs/10.1021/acs.jctc.5b00864).

369   **ACKNOWLEDGMENT**

379

380    **Figure 1.**



381

382

383

384 **Figure 2.**

A

B

385
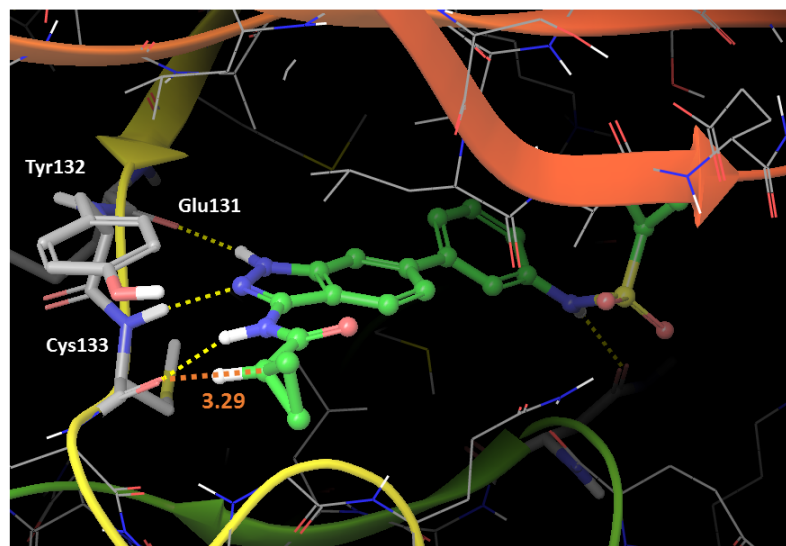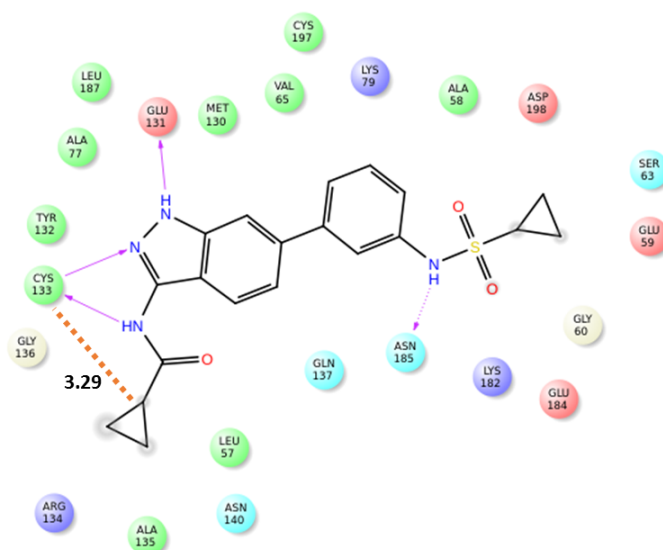
386

387    **Figure 3.**

A



B



388

## REFERENCES

1.      Cohen P, Alessi DR. Kinase drug discovery--what's next in the field? ACS Chem Biol. 2013;8(1):96-104. doi: 10.1021/cb300610s. PubMed PMID: 23276252; PubMed Central PMCID: PMCPMC4208300.

2.      Fedorov O, Muller S, Knapp S. The (un)targeted cancer kinome. Nat Chem Biol. 2010;6(3):166-9. doi: 10.1038/nchembio.297. PubMed PMID: 20154661.

3.      Uitdehaag JC, Verkaar F, Alwan H, de Man J, Buijsman RC, Zaman GJ. A guide to picking the most selective kinase inhibitor tool compounds for pharmacological validation of drug targets. Br J Pharmacol. 2012;166(3):858-76. doi: 10.1111/j.1476-5381.2012.01859.x. PubMed PMID: 22250956; PubMed Central PMCID: PMCPMC3417414.

4.      Ruegg UT, Burgess GM. Staurosporine, K-252 and UCN-01: potent but nonspecific inhibitors of protein kinases. Trends Pharmacol Sci. 1989;10(6):218-20. PubMed PMID: 2672462.

5.      Knapp S, Arruda P, Blagg J, Burley S, Drewry DH, Edwards A, et al. A public-private partnership to unlock the untargeted kinome. Nat Chem Biol. 2013;9(1):3-6. doi: 10.1038/nchembio.1113. PubMed PMID: 23238671.

6.      Arrowsmith CH, Audia JE, Austin C, Baell J, Bennett J, Blagg J, et al. The promise and peril of chemical probes. Nat Chem Biol. 2015;11(8):536-41. doi: 10.1038/nchembio.1867. PubMed PMID: 26196764.

7.      Xing L, Klug-Mcleod J, Rai B, Lunney EA. Kinase hinge binding scaffolds and their hydrogen bond patterns. Bioorg Med Chem. 2015;23(19):6520-7. doi: 10.1016/j.bmc.2015.08.006. PubMed PMID: 26358279.

8.      Sorrell FJ, Szklarz M, Abdul Azeez KR, Elkins JM, Knapp S. Family-wide Structural Analysis of Human Numb-Associated Protein Kinases. Structure. 2016;24(3):401-11. doi: 10.1016/j.str.2015.12.015. PubMed PMID: 26853940; PubMed Central PMCID: PMCPMC4780864.

9.      Liu HP, Lin YJ, Lin WY, Wan L, Sheu JJ, Lin HJ, et al. A novel genetic variant of BMP2K contributes to high myopia. J Clin Lab Anal. 2009;23(6):362-7. doi: 10.1002/jcla.20344. PubMed PMID: 19927351.

10.     Neveu G, Ziv-Av A, Barouch-Bentov R, Berkerman E, Mulholland J, Einav S. AP-2-associated protein kinase 1 and cyclin G-associated kinase regulate hepatitis C virus entry and are potential drug targets. J Virol. 2015;89(8):4387-404. doi: 10.1128/JVI.02705-14. PubMed PMID: 25653444; PubMed Central PMCID: PMC4442395.

11.     Sakurai MA, Ozaki Y, Okuzaki D, Naito Y, Sasakura T, Okamoto A, et al. Gefitinib and luteolin cause growth arrest of human prostate cancer PC-3 cells via inhibition of cyclin G-associated kinase and induction of miR-630. PLoS One. 2014;9(6):e100124. doi: 10.1371/journal.pone.0100124. PubMed PMID: 24971999; PubMed Central PMCID: PMCPMC4074034.

12.     Shi B, Conner SD, Liu J. Dysfunction of endocytic kinase AAK1 in ALS. Int J Mol Sci. 2014;15(12):22918-32. doi: 10.3390/ijms151222918. PubMed PMID: 25514244; PubMed Central PMCID: PMCPMC4284746.

432    13.    Lebakken CS, Riddle SM, Singh U, Frazee WJ, Eliason HC, Gao Y, et al.
433    Development and applications of a broad-coverage, TR-FRET-based kinase binding assay
434    platform. J Biomol Screen. 2009;14(8):924-35. doi: 10.1177/1087057109339207.
435    PubMed PMID: 19564447.

436    14.    Huse M, Kuriyan J. The conformational plasticity of protein kinases. Cell.
437    2002;109(3):275-82. PubMed PMID: 12015977.

438    15.    Kornev AP, Taylor SS. Defining the conserved internal architecture of a protein
439    kinase. Biochim Biophys Acta. 2010;1804(3):440-4. doi: 10.1016/j.bbapap.2009.10.017.
440    PubMed PMID: 19879387; PubMed Central PMCID: PMCPMC3435107.

441    16.    Chaikuad A, Keates T, Vincke C, Kaufholz M, Zenn M, Zimmermann B, et al.
442    Structure of cyclin G-associated kinase (GAK) trapped in different conformations using
443    nanobodies. Biochem J. 2014;459(1):59-69. doi: 10.1042/BJ20131399. PubMed PMID:
444    24438162; PubMed Central PMCID: PMCPMC3957475.

445    17.    Eswaran J, Bernad A, Ligos JM, Guinea B, Debreczeni JE, Sobott F, et al. Structure
446    of the human protein kinase MPSK1 reveals an atypical activation loop architecture.
447    Structure. 2008;16(1):115-24. doi: 10.1016/j.str.2007.10.026. PubMed PMID: 18184589;
448    PubMed Central PMCID: PMCPMC2194165.

449    18.    Harder E, Damm W, Maple J, Wu C, Reboul M, Xiang JY, et al. OPLS3: A Force
450    Field Providing Broad Coverage of Drug-like Small Molecules and Proteins. J Chem
451    Theory Comput. 2016;12(1):281-96. doi: 10.1021/acs.jctc.5b00864. PubMed PMID:
452    26584231.

453    19.    Still WC, Tempczyk A, Hawley RC, Hendrickson T. Semianalytical Treatment of
454    Solvation for Molecular Mechanics and Dynamics. J Am Chem Soc. 1990;112:6127-9.

455    20.    Stephens PJ, Devlin FJ, Chabalowski CF, Frisch MJ. J Phys Chem. 1994;98:11623.

456    21.    Frisch MJ, Pople JA, Binkley JS. J Chem Phys. 1984:3265.

457    22.    Stumpfe D, Bajorath J. Exploring activity cliffs in medicinal chemistry. J Med
458    Chem. 2012;55(7):2932-42. doi: 10.1021/jm201706b. PubMed PMID: 22236250.

459    23.    Liang J, Tsui V, Van Abbema A, Bao L, Barrett K, Beresini M, et al. Lead
460    identification of novel and selective TYK2 inhibitors. Eur J Med Chem. 2013;67:175-87.
461    doi: 10.1016/j.ejmech.2013.03.070. PubMed PMID: 23867602.

462    24.    Menet CJ, Fletcher SR, Van Lommen G, Geney R, Blanc J, Smits K, et al.
463    Triazolopyridines as selective JAK1 inhibitors: from hit identification to GLPG0634. J Med
464    Chem. 2014;57(22):9323-42. doi: 10.1021/jm501262q. PubMed PMID: 25369270.

465    25.    Li X, Shen J, Tan L, Zhang Z, Gao D, Luo J, et al. Design and synthesis of N-(4-
466    aminopyridin-2-yl)amides as B-Raf(V600E) inhibitors. Bioorg Med Chem Lett.
467    2016;26(12):2760-3. doi: 10.1016/j.bmcl.2016.04.076. PubMed PMID: 27155899.

468    26.    Talele TT. The "Cyclopropyl Fragment" is a Versatile Player that Frequently
469    Appears in Preclinical/Clinical Drug Molecules. J Med Chem. 2016;59(19):8712-56. doi:
470    10.1021/acs.jmedchem.6b00472. PubMed PMID: 27299736.

471    27.    Galano A, Alvarez-Idaboy J, Vivier-Bunge A. Non-alkane behavior of cyclopropane
472    and its derivatives: characterization of unconventional hydrogen bond interactions.
473    Theor Chem Account. 2007;118:597-606.

474    28.    Witherington J, Bordas V, Gaiba A, Naylor A, Rawlings AD, Slingsby BP, et al. 6-
475    heteroaryl-pyrazolo[3,4-b]pyridines: potent and selective inhibitors of glycogen

476   synthase kinase-3 (GSK-3). Bioorg Med Chem Lett. 2003;13(18):3059-62. PubMed PMID:
477   12941333.

478   29.   Chang CE, Chen W, Gilson MK. Ligand configurational entropy and protein
479   binding. Proc Natl Acad Sci U S A. 2007;104(5):1534-9. doi: 10.1073/pnas.0610494104.
480   PubMed PMID: 17242351; PubMed Central PMCID: PMCPMC1780070.

481   30.   Davis MI, Hunt JP, Herrgard S, Ciceri P, Wodicka LM, Pallares G, et al.
482   Comprehensive   analysis   of   kinase   inhibitor   selectivity.   Nat   Biotechnol.
483   2011;29(11):1046-51. doi: 10.1038/nbt.1990. PubMed PMID: 22037378.

484   31.   Fabian MA, Biggs WH, 3rd, Treiber DK, Atteridge CE, Azimioara MD, Benedetti
485   MG, et al. A small molecule-kinase interaction map for clinical kinase inhibitors. Nat
486   Biotechnol. 2005;23(3):329-36. doi: 10.1038/nbt1068. PubMed PMID: 15711537.

487   32.   Derewenda ZS.   Rational   protein   crystallization   by   mutational   surface
488   engineering.   Structure.   2004;12(4):529-35.   doi:   10.1016/j.str.2004.03.008.   PubMed
489   PMID: 15062076.

490   33.   Newman J. Novel buffer systems for macromolecular crystallization. Acta
491   crystallographica Section D, Biological crystallography. 2004;60(Pt 3):610-2. doi:
492   10.1107/S0907444903029640. PubMed PMID: 14993709.

493   34.   Chaikuad A, Knapp S, von Delft F. Defined PEG smears as an alternative approach
494   to enhance the search for crystallization conditions and crystal-quality improvement in
495   reduced screens. Acta crystallographica Section D, Biological crystallography. 2015;71(Pt
496   8):1627-39.   doi:   10.1107/S1399004715007968.   PubMed   PMID:   26249344;   PubMed
497   Central PMCID: PMC4528798.

498   35.   Kabsch W. Xds. Acta crystallographica Section D, Biological crystallography.
499   2010;66(Pt 2):125-32.   doi:   10.1107/S0907444909047337.   PubMed   PMID:   20124692;
500   PubMed Central PMCID: PMC2815665.

501   36.   Winn MD, Ballard CC, Cowtan KD, Dodson EJ, Emsley P, Evans PR, et al. Overview
502   of the CCP4 suite and current developments. Acta crystallographica Section D, Biological
503   crystallography.   2011;67(Pt   4):235-42.   doi:   10.1107/S0907444910045749.   PubMed
504   PMID: 21460441; PubMed Central PMCID: PMC3069738.

505   37.   McCoy AJ, Grosse-Kunstleve RW, Adams PD, Winn MD, Storoni LC, Read RJ.
506   Phaser crystallographic software. Journal of applied crystallography. 2007;40(Pt 4):658-
507   74.   doi:   10.1107/S0021889807021206.   PubMed   PMID:   19461840;   PubMed   Central
508   PMCID: PMC2483472.

509   38.   Cowtan K. The Buccaneer software for automated model building. 1. Tracing
510   protein chains. Acta crystallographica Section D, Biological crystallography. 2006;62(Pt
511   9):1002-11. doi: 10.1107/S0907444906022116. PubMed PMID: 16929101.

512   39.   Zhang KY, Cowtan K, Main P. Combining constraints for electron-density
513   modification. Methods in enzymology. 1997;277:53-64. PubMed PMID: 18488305.

514   40.   Emsley P, Lohkamp B, Scott WG, Cowtan K. Features and development of Coot.
515   Acta crystallographica Section D, Biological crystallography. 2010;66(Pt 4):486-501. doi:
516   10.1107/S0907444910007493.   PubMed   PMID:   20383002;   PubMed   Central   PMCID:
517   PMC2852313.

518   41.   Chen VB, Arendall WB, 3rd, Headd JJ, Keedy DA, Immormino RM, Kapral GJ, et al.
519   MolProbity:   all-atom   structure   validation   for   macromolecular   crystallography.   Acta

520    crystallographica Section D, Biological crystallography. 2010;66(Pt 1):12-21. doi:
521    10.1107/S0907444909042073. PubMed PMID: 20057044; PubMed Central PMCID:
522    PMC2803126.
523    42.    Schrödinger Release 2016-3: MacroModel, Schrödinger, LLC New York, NY, 2016.
524    43.    Schrödinger Release 2016-4: Jaguar, Schrödinger, LLC, New York, NY, 2016.
525

526